Theoretical study of the electronic structure of hafnium (Hf, $Z = 72$) and rutherfordium (Rf, $Z = 104$) atoms and their ions: Energy levels and hyperfine-structure constants

Saleh O. Allehabi, V. A. Dzuba, and V. V. Flambaum
School of Physics, University of New South Wales, Sydney 2052, Australia

(Received 26 September 2021; accepted 8 November 2021; published 18 November 2021)

Energy levels, magnetic dipole, and electric quadrupole hyperfine structure of the superheavy element rutherfordium (Rf, $Z = 104$) and its first three ions are calculated using a combination of the configuration interaction, linearized coupled-cluster single-doubles, and many-body perturbation theory techniques. The results are to be used in future interpretations of the measurements in terms of nuclear magnetic dipole and electric quadrupole moments. To have a guide on the accuracy of the study, we perform similar calculations for hafnium (Hf, $Z = 72$) and its ions. Hf is a lighter analog of Rf with a similar electronic structure. Good agreement with the experiment for Hf and with available previous calculations of the energy levels of Rf is demonstrated.

DOI: 10.1103/PhysRevA.104.052811

I. INTRODUCTION

The study of the hyperfine structure (hfs) of the superheavy elements ($Z > 100$) is a way of obtaining important information about their nuclear structure. The measurements accompanied by atomic calculations lead to extractions of nuclear magnetic dipole and electric quadrupole moments. This serves as a test of nuclear theory leading to more reliable predictions of nuclear properties and helping in the search for the hypothetical *stability island* [1–5]. The heaviest element so far where such a study was performed is nobelium (No, $Z = 102$) [6–8]. The hfs was measured for ^{253}No isotope in the strong electric dipole transition between ground $^1S_0$ and excited $^1P^o_1$ state. In addition, isotope shift was measured for the ^{252,253,254}No isotopes. Similar measurements are now planned for lawrencium (Lr, $Z = 103$) [9]. Hopefully, rutherfordium (Rf, $Z = 104$) is next in line.

Most of the synthesized isotopes of Rf have odd neutron numbers [10], meaning that they have a nonzero nuclear spin and that their energy levels have hyperfine structures. The spectrum of electronic states of Rf was studied theoretically before [11–13], revealing several electric dipole transitions suitable for the measurements.

In the present work, we perform calculations of energy levels, magnetic dipole, and electric quadrupole hyperfine structure (hfs) of neutral Rf and Hf and their first three ions. The main purpose of the work is to obtain the values of the hfs matrix elements needed for the interpretation of future measurements. The energy levels are obtained as a byproduct; they are also useful for assessing the accuracy of the calculations.

We use a combination of the linearized single-double coupled-cluster method with the configuration interaction technique, the CI+SD method [14]. Calculations for Hf are performed to test the accuracy of the predictions for Rf. Hf is a lighter analog of Rf with a similar electronic structure. Good agreement with the experiment for Hf and with previous calculations of the energy levels of Rf is demonstrated. This opens a way for the interpretation of future measurements in terms of the nuclear magnetic dipole and electric quadrupole moments.

II. METHOD OF CALCULATION

A. Calculation of energy levels

For all considered systems, calculations start for the relativistic Hartree-Fock (RHF) procedure for the closed-shell core (Hf V and Rf V). This corresponds to the use of the V^{N-M} approximation [15]. Here $N = Z$ is the total number of electrons in a neutral atom, and M is the number of valence electrons ($M = 4$ for Hf I and Rf I). The RHF Hamiltonian has the form,

$$\hat{H}^{\rm RHF} = c\alpha\hat{p} + (\beta - 1)mc^2 + V_{\rm nuc}(r) + V_{\rm core}(r), \quad (1)$$

where c is the speed of light, α and β are the Dirac matrices, $\hat{p}$ is the electron momentum, m is the electron mass, $V_{\rm nuc}$ is the nuclear potential obtained by integrating Fermi distribution of nuclear charge density, and $V_{\rm core}(r)$ is the self-consistent RHF potential created by the electrons of the closed-shell core.

After the self-consistent procedure for the core is completed, the full set of single-electron states is generated using the B-spline technique [16,17]. The basis states are linear combinations of B splines, which are the eigenstates of the RHF Hamiltonian (1). We use 40 B splines of the order 9 in a box that has a radius $R_{\rm max} = 40a_B$ with the orbital angular momentum $0 \leqslant l \leqslant 6$. These basis states are used for solving the linearized single-double couple-cluster (SD) equations and for generating many-electron states for the configuration interaction (CI) calculations. By solving the SD equations first for the core and then for the valence states, we obtain correlation operators Σ_1 and Σ_2 [14]. Σ_1 is a one-electron operator which is responsible for correlation interaction between a particular valence electron and the core. Σ_2 is a two-electron operator that can be understood as screening of Coulomb interaction between a pair of valence electrons by core electrons. These

Σ operators can be used in the subsequent CI calculations for atoms with several valence electrons to account for the core-valence and core-core correlations. Solving the SD equations for valence states also gives energies of the single-electron states for the system with one external electron above closed shells. Note that there is a small difference in the SD equations intended for obtaining these energies compared to those intended for further use in the CI calculations. In the latter case, one particular term should be removed from the SD equations since its contribution is included via the CI calculations (see Ref. [14] for details). However, the contribution of this term is small, and the difference in the SD equations can be neglected.

The CI equations,

$$\langle a|\hat{H}^{\rm CI}|b\rangle - E\delta_{ab} = 0, \tag{2}$$

have the CI Hamiltonian, which includes Σ_1 and Σ_2,

$$\hat{H}^{\rm CI} = \sum_{i=1}^{M}(\hat{H}^{\rm RHF} + \Sigma_1)_i + \sum_{i<j}^{M}\left(\frac{e^2}{|r_i - r_j|} + \Sigma_{2ij}\right). \tag{3}$$

a and b in (2) are many-electron single determinant basis states which are constructed by exciting one or two electrons from one or more reference configuration(s) and then building from these configurations the states of definite values of the total momentum J. M in (3) is the number of valence electrons. In our cases $M = 1, 2, 3, 4$. The case of one external electron is a special one. It has no terms of the second line in the CI Hamiltonian (3). Taking into account that single-electron basis states are eigenstates of the RHF Hamiltonian (1), the CI eigenvalue problem is reduced to diagonalization of the Σ_1 matrix,

$$\langle i|\Sigma_1|j\rangle - E\delta_{ij} = 0. \tag{4}$$

Here i and j are single-electron basis states. Note that in spite of significant simplifications of the CI equations for $M = 1$, there is no need for the modification of the computer code. For $M = 1$ Eqs. (2) and (4) are equivalent.

There is an alternative way to perform the calculations for systems with one external electron. One can find the energies and wave functions of the valence states by solving the RHF-like equations for an external electron in which the correlation potential Σ_1 is included:

$$(\hat{H}^{\rm RHF} + \Sigma_1 - \epsilon_v)\psi_v = 0. \tag{5}$$

Here index v numerate states of an external electron, wave functions ψ_v are usually called the Brueckner orbitals (BO) [18], and the energies ϵ_v and wave functions ψ_v include correlation corrections. The BO can be used to calculate matrix elements, in particular, for the hfs (see below). Comparing two ways of the calculations is an important test of the accuracy. It is especially valuable when there is a lack of experimental data, which is the case of the present work.

The meaning of the Σ_1 operator is the same in the CI and BO equations [Eqs. (4) and (5)]. However, the Σ_1 operator, which comes from the SD calculations as a set of matrix elements between single-electron states, cannot be directly used in (5) since here we need the operator in the coordinate representation. Therefore, we calculate the Σ_1 for the BO in the second order of the many-body perturbation theory (see Fig. 1). A particular class of the higher-order correlations is included by solving Eq. (5) iteratively. It includes contributions $\sim\Sigma_1^2$, Σ_1^3, etc. In the end, the two ways of calculations are sufficiently different to be a good test of accuracy.

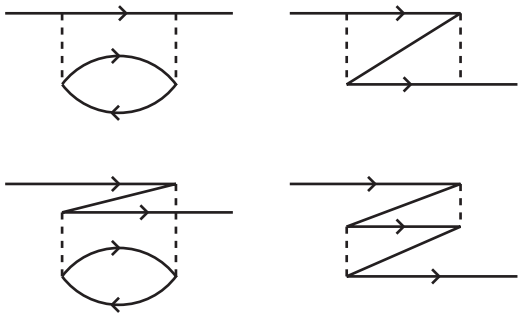

FIG. 1. Four diagrams for the second-order correlation operator Σ_1.

B. The CIPT method

It is very well known that the size of the CI matrix grows exponentially with the number of valence electrons. In the present work, we have up to four valence electrons (in neutral Hf and Rf), leading to the huge size of the CI matrix, the number of lines in (2) $\sim 10^6$. Dealing with a matrix of this size requires significant computer power. However, it can be reduced by orders of magnitude for the cost of some sacrifices in the accuracy of the result. To do this, we use the CIPT method [19] (configuration interaction with perturbation theory). The idea is to neglect off-diagonal matrix elements between high-energy states in the CI matrix (since in the perturbation theory approach, such matrix elements appear in higher orders). Then the CI matrix equation [Eq. (2)] can be written in a block form,

$$\begin{pmatrix} A & B \\ C & D \end{pmatrix}\begin{pmatrix} X \\ Y \end{pmatrix} = E_a\begin{pmatrix} X \\ Y \end{pmatrix}. \tag{6}$$

Here block A corresponds to low-energy states, block D corresponds to high-energy states, and blocks B and C correspond to cross terms. Note that since the total CI matrix is symmetric, we have $C = B'$, i.e., $c_{ij} = b_{ji}$. Vectors X and Y contain the coefficients of expansion of the valence wave function over the single-determinant many-electron basis functions,

$$\Psi(r_1, \ldots, r_M) = \sum_{i=1}^{N_1} X_i\Phi_i(r_1, \ldots, r_M) + \sum_{j=1}^{N_2} Y_j\Phi_j(r_1, \ldots, r_M). \tag{7}$$

Here M is the number of valence electrons, N_1 is the number of low-energy basis states, and N_2 is the number of high-energy basis states.

We neglect off-diagonal matrix elements in block D. Finding Y from the second equation of (6) leads to

$$Y = (E_aI - D)^{-1}CX. \tag{8}$$

Substituting Y to the first equation of (6) leads to

$$[A + B(E_aI - D)^{-1}C]X = E_vX, \tag{9}$$

TABLE I. The number of configurations and the size of the effective CI matrix for Hf and Rf. NNC is the number of nonrelativistic configurations, NRC is the number of relativistic configurations, and N_1 is the corresponding number of states with given J^p.

J^p	NNC	NRC	N_1
1^+	80	364	726
2^+	80	364	987
3^+	80	364	968
4^+	80	364	784
1^-	60	259	470
2^-	60	259	605
3^-	60	259	566

where I is the unit matrix. Neglecting the off-diagonal matrix elements in D leads to a very simple structure of the $(E_a I - D)^{-1}$ matrix, $(E_a I - D)^{-1}_{ik} = \delta_{ik}/(E_a - E_k)$, where $E_k = \langle k|H^{\rm CI}|k\rangle$ (see [19] for more details). Equation (9) gives the same solution as Eq. (6) if the energy parameter E_a in the left-hand side of (9) has the same value as the solution E_v. Since the value of E_v is not known in advance, we use an iterative procedure, $E_a^{(n)} = E_v^{(n-1)}$, where n is iteration number. On first iteration one can use a solution of the simplified equation $AX = E_a X$ or use some guess energy. In most cases less than 10 iterations is sufficient for full convergence.

The relative sizes of blocks A and D can be varied in the calculations in search of a reasonable compromise between the accuracy of the results and the computer power needed to obtain them. In our current calculations, the number of lines in (9) is $\sim 10^3$.

Note that the CI matrix is different for every combination of the value of the total angular momentum J and the parity of the states (J^p). Therefore, the choice of the N_1 parameter (i.e., the size of the effective CI matrix) should be done separately for every J^p. In doing so we follow the rule that all states of the same configuration should be treated equally, either as low-energy or high-energy states. Since for every given configuration the number of states with different values of J is different, the values of N_1 are also different for every J^p. The search for a compromise between the size of the effective CI matrix and the accuracy of the results is also done separately for every J^p. Table I shows the parameters used in the present calculations. The only external parameter chosen "by hands" is the number of nonrelativistic configurations. The values of other parameters are calculated. For example, one nonrelativistic configuration $7s^2 6d^2$ corresponds to three relativistic configurations: $7s^2 6d^2_{3/2}$, $7s^2 6d_{3/2} 6d_{5/2}$, and $7s^2 6d^2_{5/2}$. The total number of states included in the calculations, $N_1 + N_2$, also varies with J^p being about 10^6.

C. Calculation of hyperfine structure

To calculate hfs, we use the time-dependent Hartree-Fock (TDHF) method, which is equivalent to the well-known random-phase approximation (RPA). The RPA equations are the following:

$$(\hat{H}^{\rm RHF} - \epsilon_c)\delta\psi_c = -\big(\hat{f} + \delta V^f_{\rm core}\big)\psi_c, \tag{10}$$

where $\hat{f}$ is an operator of an external field (an external electric field, nuclear magnetic dipole, or electric quadrupole fields). Index c in (10) numerates states in the core, ψ_c is a single-electron wave function of the state c in the core, $\delta\psi_c$ is the correction to this wave function caused by an external field, and $\delta V^f_{\rm core}$ is the correction to the self-consistent RHF potential caused by changing of all core states. The nucleus is assumed to be a sphere with a uniform distribution of the nuclear electric quadrupole moment and the nuclear magnetic dipole moment. Equation (10) is solved self-consistently for all states in the core. As a result, an effective operator of the interaction of valence electrons with an external field is constructed as $\hat{f} + \delta V^f_{\rm core}$. The energy shift of a many-electron state a, which is a solution of the CI equations [Eq. (2)], is given by

$$\delta\epsilon_a = \langle a|\sum_{i=1}^{M}\big(\hat{f} + \delta V^f_{\rm core}\big)_i|a\rangle. \tag{11}$$

When the wave function for the valence electrons comes as a solution of Eq. (9), Eq. (11) is reduced to

$$\delta\epsilon_a = \sum_{ij} x_i x_j \langle\Phi_i|\hat{H}^{\rm hfs}|\Phi_j\rangle, \tag{12}$$

where $\hat{H}^{\rm hfs} = \sum_{i=1}^{M}(\hat{f} + \delta V^f_{\rm core})_i$. For better accuracy of the results, the full expansion (7) might be used. Then it is convenient to introduce a new vector Z, which contains both X and Y, $Z \equiv \{X, Y\}$. Note that the solution of (9) is normalized by the condition $\sum_i x_i^2 = 1$. The normalization condition for the total wave function (7) is different, $\sum_i x_i^2 + \sum_j y_j^2 \equiv \sum_i z_i^2 = 1$. Therefore, when X is found from (9), and Y is found from (8), both vectors should be renormalized. Then the hfs matrix element is given by the expression, which is similar to (12) but has many more terms,

$$\delta\epsilon_a = \sum_{ij} z_i z_j \langle\Phi_i|\hat{H}^{\rm hfs}|\Phi_j\rangle. \tag{13}$$

In the case of one external electron, the calculations can also be done using the BO,

$$\delta\epsilon_v = \big\langle v\big|\hat{f} + \delta V^f_{\rm core}\big|v\big\rangle. \tag{14}$$

Here v stands for a solution of Eq. (5). Energy shifts (11) and (14) are used to calculate hfs constants A and B using textbook formulas:

$$A_a = \frac{g_I \delta\epsilon_a^{(A)}}{\sqrt{J_a(J_a+1)(2J_a+1)}}, \tag{15}$$

and

$$B_a = -2Q\delta\epsilon_a^{(B)}\sqrt{\frac{J_a(2J_a-1)}{(2J_a+3)(2J_a+1)(J_a+1)}}. \tag{16}$$

Here $\delta\epsilon_a^{(A)}$ is the energy shift (11) or (14) caused by the interaction of atomic electrons with the nuclear magnetic moment μ, $g_I = \mu/I$, I is nuclear spin; $\delta\epsilon_a^{(B)}$ is the energy shift (11) or (14) caused by the interaction of atomic electrons with the nuclear electric quadrupole moment Q [Q in (16) is measured in barns].

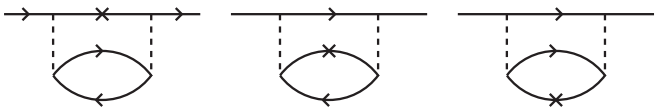

FIG. 2. Sample SR diagrams corresponding to the first diagram in Fig. 1. The cross stands for the hfs operator. It goes to all internal lines of all four diagrams for the Σ_1 operator.

D. Further corrections to the hyperfine structure

Using Eq. (12) is the fastest way of calculating hfs for many-electron atoms. Sometimes it gives pretty accurate results, within ∼10% of the experimental values. This is usually the case when the hfs comes mostly from contributions of the s and p states. In our case, the contribution of the s states is suppressed because, in the leading configurations ($6s^25d^2$ and $6s^25d6p$), the $6s$ electrons are from the closed subshell and do not contribute to the hfs. This means that further corrections to the hfs matrix elements should be considered. Equation (12) can still be used to identify states with large hfs. The accuracy of the calculations is likely to be higher for such states. This is because the small value of the hfs often comes as a result of strong cancellations between different contributions leading to poor accuracy of the results.

There are at least three classes of the higher-order corrections to the hfs matrix elements: (a) Contribution of the higher states (HS). This is the difference between (13) and (12). (b) Corrections to the single-electron matrix elements caused by the correlation operator Σ_1. This includes *the structure radiation* (SR) when the hfs operator is inside of the Σ_1 operator (see Fig. 2) and the self-energy correction when the hfs operator is outside of the Σ_1 operator (see Fig. 3) (see also [20,21]). (c) Two-particle correction [20,21], which is a correction to the Coulomb interaction between valence electrons caused by the hfs interaction (see Fig. 4).

To study the corrections to the single-electron matrix elements, it is convenient to have a system with one external electron above closed shells where experimental data are available for a range of valence states. The $^{135}Ba^+$ ion is a good example of such a system. Table II presents a comparison with the measured magnetic dipole hfs constants of $^{135}Ba^+$, calculated in different approximations. The RHF (relativistic Hartree-Fock) column corresponds to using Eq. (14) in which the valence state $|v\rangle$ is a Hartree-Fock orbital and the core polarization correction $\delta V^f_{\rm core}$ is absent. In the RPA column the CP correction is added, BORPA corresponds to using the BO in (14), and the BORPA rescaled is the same but the BO calculated with rescaled correlation operator $\lambda\Sigma_1$; the rescaling parameter λ is chosen to fit the experimental energies. The SR column is the structure radiation (Fig. 2), and the *total* column is the sum of the previous two columns.

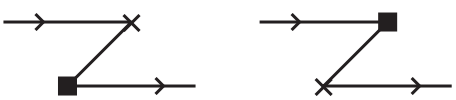

FIG. 3. Self-energy diagrams. The cross stands for the hfs operator, and the black box stands for the correlation operator Σ_1 (see Fig. 1).

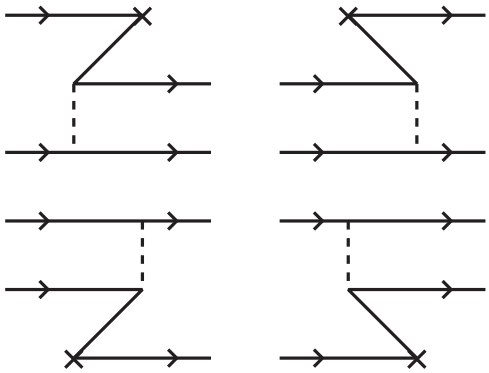

FIG. 4. Two-particle correction to the many-electron matrix element of the hfs interaction. The cross stands for the hfs operator, and the dashed line is the Coulomb interaction.

The last column presents the experimental hfs constants from Ref. [22,23]. The table shows that all considered corrections are important, and including them all leads to accurate results in most cases. Therefore, all these corrections should be included in the calculations for many-electron atoms via correcting single-electron matrix elements. The inclusion of the CP and SR corrections is straightforward, but the inclusion of correlations like in the BO needs some clarification. The CI Hamiltonian (3) does include the correlation operator Σ_1 leading to the mixing of the states above the core and forming orbitals similar to BO. No core states are involved in this mixing. On the other hand, the BO found by solving Eq. (5) can be written in the first order of Σ_1 as

$$\psi_v^{\rm BO} = \sum_i |i\rangle \frac{\langle i|\Sigma_1|v\rangle}{E_v - E_i}. \tag{17}$$

Here summation goes over the complete set of the single-electron Hartree-Fock states, including states in the core. The self-energy (SE) terms (Fig. 3) are needed to account for this missed summation over the core states in the CI calculations. Table II shows that the considered approximation gives very accurate results for the hfs of the s and p state, while the results for the d states are less accurate. Furthermore, the relative difference between theory and experiment for $d_{3/2}$ states is about two times smaller than for the $d_{5/2}$ states. This means that while considering the hfs of many-electron atoms in which the values of the hfs constants come mostly from the contribution of the d states (like Hf and Rf), it is preferable to consider states in which the contribution of the

TABLE II. Magnetic dipole hfs constants of $^{135}Ba^+$ (MHz) calculated in different approximations.

State	RHF	RPA	BORPA	BORPA rescaled	SR	Total	Expt. [22,23]
$6s_{1/2}$	2603	3090	3815	3654	−63	3591	3593
$6p_{1/2}$	440	530	691	659	5	664	665
$6p_{3/2}$	64	105	134	129	−16	113	113
$5d_{3/2}$	115	133	165	161	27	188	170
$5d_{5/2}$	46	−50	−47	−48	35	−13	−10.7

$d_{3/2}$ states dominates over the contribution of the $d_{5/2}$ states. The accuracy of the calculations is likely to be higher for these states. To identify such states, we need to do the analysis of the partial contributions to the hfs of the many-electron atoms. We will further discuss the matter in Sec. III B.

III. RESULTS

A. Energy levels of Hf, Rf, and their ions

Calculated energy levels of Hf and its first three ions are presented in Table III and are compared with the experiment. Good agreement between the sets of data indicates that applied approximation is sufficiently accurate to proceed to the calculations of the hyperfine structure. Energy levels of Hf and Hf^+ were calculated before (see, e.g., [13] for Hf and [24] for Hf^+). We do not make a direct comparison between the results because to assess the accuracy of the method, it is sufficient to compare the result with the experiment. However, it is useful to understand the reasons for some differences in our results with the results of previous calculations of Ref. [13]. Some energy levels calculated in [13] are closer to the experiment than in the present work (e.g., low energy states); others (e.g., some high energy states) are closer to the experiment in our present work. The main reason for the differences is the use of the different versions of the CI+SD method. The method of Ref. [25] was used in Ref. [13], while in the present work, we use the method of Ref. [14]. Another reason for the differences comes from the fact that in the present work we do not include radiative corrections. This is because we focus mostly on the hyperfine structure. However, the method of inclusion of the radiative corrections developed in Ref. [26] and used in Ref. [13] is applicable for the energy levels and transition amplitudes but not applicable for the singular operators like the operators of hfs. Finally, in the present work, we use the CIPT technique to get a huge gain in sensitivity while making some sacrifices in accuracy (see Sec. II B for details). This approach was not used in previous works, and this is another reason for some differences in the results.

Calculated energy levels of Rf and its first three ions are presented in Table IV and compared with other calculations. Energy levels of neutral Rf were calculated in a number of earlier works [11–13,27], and energy levels of Rf+ were calculated in Refs. [11,13]; only the ionization potential (IP) of Rf III and Rf IV were reported before [13,27,28]. The origin of the differences in the energies of Rf in our present work and earlier work of Ref. [13] is the same as for Hf; see discussion above.

As can be seen from the table, the results of the present calculations for Rf and Rf^+ are in excellent agreement with previous studies; the difference between the energies of earlier works and present results for Rf is within 300 cm^{-1} for a majority of energy levels, and it is up to ∼1000 cm^{-1} for some states. The difference for Rf^+ is within ∼2000 cm^{-1}, and for some states it is significantly smaller.

The ionization potentials for Rf III and Rf IV have been calculated, and the results obtained are 192 367 cm^{-1} and 257 396 cm^{-1}, respectively. Those results are compared with experiment and other theoretical studies. In Ref. [28], the measured results achieved for the IP are 191 960 cm^{-1} and 257 290 cm^{-1} for Rf III and Rf IV, respectively; and in

TABLE III. Excitation energies (E, cm^{-1}) for some low states of Hf I, Hf II, Hf III, and Hf IV.

No.	Conf.	Term	J	Present (CI+SD)	Expt.
		Hf I			[29]
1	$5d^26s^2$	^3F	2	0	0
2	$5d^26s^2$	^3F	3	2114	2356.68
3	$5d^26s^2$	^3F	4	4148	4567.64
4	$5d^26s^2$	^1D	2	4799	5638.62
5	$5d^26s^2$	^3P	1	5063	6572.54
6	$5d^26s^2$	^3P	2	9026	8983.75
7	$5d6s^26p$	$^1D^o$	2	10 634	10 508.88
8	$5d^26s^2$	^1G	4	10 402	10 532.55
9	$5d6s^26p$	$^3D^o$	1	14 042	14 017.81
10	$5d^36s$	^5F	1	12 469	14 092.26
11	$5d6s^26p$	$^3F^o$	2	14 092	14 435.12
12	$5d6s^26p$	$^3F^o$	3	14 545	14 541.66
13	$5d^36s$	^5F	2	12 625	14 740.67
14	$5d^36s$	^5F	3	13 181	15 673.32
15	$5d6s^26p$	$^3D^o$	2	15 706	16 163.35
16	$5d^36s$	^5F	4	14 050	16 766.60
17	$5d^26s6p$	$^5G^o$	2	18 234	18 011.04
18	$5d6s^26p$	$^3P^o$	1	17 969	18 143.39
19	$5d6s^26p$	$^3F^o$	4	16 485	18 224.97
20	$5d6s^26p$	$^3D^o$	3	17 824	18 381.50
21	$5d^26s6p$	$^5G^o$	3	19 148	19 292.68
22	$5d6s^26p$	$^3P^o$	2	19 490	19 791.29
23	$5d^36s$	^5P	1	18 363	20 784.87
24	$5d^36s$	^5P	2	19 085	20 908.43
		Hf II			[29]
1	$5d6s^2$	^2D	3/2	0	0
2	$5d6s^2$	^2D	5/2	3054	3050.88
3	$5d^26s$	^4F	3/2	3578	3644.65
4	$5d^26s$	^4F	5/2	4312	4904.85
5	$5d^26s$	^4F	7/2	5330	6344.34
6	$5d^26s$	^4F	9/2	8039	8361.76
7	$5d^26s$	^4P	1/2	11 675	11 951.70
8	$5d^26s$	^2F	5/2	11 783	12 070.46
9	$5d^26s$	^4P	3/2	11 781	12 920.94
10	$5d^26s$	^4P	5/2	12 581	13 485.56
11	$5d^26s$	^4D	3/2	13 836	14 359.42
12	$5d^26s$	^2F	7/2	14 410	15 084.26
13	$5d6s6p$	$^4F^o$	3/2	28 580	28 068.79
14	$5d6s6p$	$^4D^o$	1/2	29 249	29 160.04
15	$5d6s6p$	$^4F^o$	5/2	29 759	29 405.12
16	$5d6s6p$	$^4D^o$	3/2	31 903	31 784.16
		Hf III			[30]
1	$5d^2$	^3F	2	0	0
2	$5d6s$	^3D	2	2572	3039.7
3	$5d^2$	^3F	3	1944	3288.7
4	$5d^2$	^1D	2	5212	5716
5	$5d^2$	^3F	4	5598	6095.1
6	$5d6s$	^3D	3	6443	6881.6
7	$5d^2$	^3P	2	11 909	12 493.2
		Hf IV			[30]
1	$4f^{14}5d$	^2D	3/2	0	0
2	$4f^{14}5d$	^2D	5/2	4721	4692
3	$4f^{14}6s$	^2S	1/2	17 530	18 380
4	$4f^{14}6p$	$^2P^o$	1/2	66 611	67 039

TABLE III. (*Continued.*)

No.	Conf.	Term	J	Present (CI+SD)	Expt.
5	$4f^{14}6p$	$^2P^o$	3/2	76 232	76 614
6	$4f^{14}7s$	^2S	1/2	140 329	140 226

Ref. [27], the calculated results obtained are 192 301 cm^{-1} and 257 073 cm^{-1}, respectively. All these values are in excellent agreement with the results of the present work. For Rf III, the difference is just 407 cm^{-1} compared with [28] and 66 cm^{-1} compared with [27]; and for Rf IV, the variation is just 106 cm^{-1} compared with [28] and 323 cm^{-1} compared with [27]. This is well inside of the error bars of this work.

Comparison of the spectra of Rf and its ions (Table IV) with the spectra of Hf and its ions (Table III) show many similarities and some differences. The most prominent difference is the difference in the ground-state configurations of the double and triple ionized ions. This difference comes from the relativistic effects, which pull s electrons closer to the nucleus, reversing the order of the $7s$ and $6d$ states of the Rf ions on the energy scale compared to the $6s$ and $5d$ states of the Hf ions.

TABLE IV. Excitation energies (E, cm^{-1}) for some low states of Rf I, Rf II, Rf III, and Rf IV.

No.	Conf.	Term	J	Present (CI+SD)	Other Cal.		
		Rf I			[11]	[12]	[13]
1	$7s^26d^2$	^3F	2	0	0	0	0
2	$7s^27p6d$	$^3F^o$	2	2737	2210	3923	2547
3	$7s^26d^2$	^3F	3	4259	4855	4869	4904
4	$7s^26d^2$	^3P	2	6873	7542	8704	7398
5	$7s^26d^2$	^3P	1	7502	8776	10 051	8348
6	$7s^26d^2$	^3F	4	7836	7542	8597	8625
7	$7s^27p6d$	$^3D^o$	1	8028	8373	9201	8288
8	$7s^27p6d$	$^3D^o$	2	11 235	10 905	12 889	11 273
9	$7s^27p6d$	$^3F^o$	3	11 328	11 905	12 953	11 390
10	$7s^27p6d$	$^1D^o$	2	13 811	–	–	14 403
11	$7s^26d^2$	^1D	2	13 841	–	–	13 630
12	$7s^26d^2$	^1G	4	14 040	–	–	14 476
13	$7s^27p6d$	$^3P^o$	1	16 017	–	–	16 551
14	$7s^27p6d$	$^3D^o$	3	17 367	–	–	18 029
15	$7s^27p6d$	$^3F^o$	4	19 979	–	–	20 477
16	$7s6d^27p$	$^5G^o$	2	20 371	–	–	20 347
17	$7s6d^3$	^5F	1	20 626	–	–	21 552
18	$7s^27p6d$	$^3P^o$	2	21 031	–	–	21 480
19	$7s6d^3$	^5F	2	21 512	–	–	23 079
20	$7s6d^27p$	$^5G^o$	3	22 941	–	–	23 325
21	$7s6d^3$	^5F	3	23 002	–	–	25 432
22	$7s^27p6d$	$^1F^o$	3	23 965	–	–	24 634
23	$7s6d^3$	^5F	4	25 231	–	–	–
24	$7s6d^27p$	$^5F^o$	1	25 821	–	–	–
		Rf II			[11]	[24]	
1	$7s^26d$	^2D	3/2	0	0	0	–
2	$7s^26d$	^2D	5/2	7026	7444	5680	–
3	$7s6d^2$	^4F	3/2	15 030	–	15 678	–
4	$7s6d^2$	^4F	5/2	16 817	–	17 392	–
5	$7s^27p$	$^2P^o$	1/2	19 050	19 390	16 657	–
6	$7s6d^2$	^4P	1/2	23 701	–	24 615	–
7	$7s6d^2$	^4D	5/2	25 392	–	26 565	–
8	$7s6d^2$	^4P	3/2	25 561	–	26 648	–
9	$7s6d^2$	^4D	3/2	28 940	–	29 983	–
10	$7s7p6d$	$^4F^o$	3/2	30 264	–	27 846	–
11	$7s6d^2$	^2P	1/2	31 238	–	32 550	–
12	$7s7p6d$	$^4F^o$	5/2	33 320	–	31 031	–
13	$7s^27p$	$^2P^o$	3/2	33 621	35 513	31 241	–
14	$7s7p6d$	$^4D^o$	1/2	37 378	–	36 156	–
15	$7s7p6d$	$^2P^o$	3/2	40 015	–	38 814	–
16	$7s7p6d$	$^4D^o$	5/2	40 640	–	42 410	–
		Rf III					
1	$7s^2$	^1S	0	0	–	–	–
2	$7s6d$	^3D	1	8526	–	–	–
3	$7s6d$	^3D	2	9945	–	–	–
4	$7s6d$	^3D	3	16 878	–	–	–
5	$7s6d$	^1D	2	19 165	–	–	–
6	$6d^2$	^3F	2	24 371	–	–	–
7	$6d^2$	^3F	3	28 326	–	–	–
		Rf IV					
1	$5f^{14}7s$	^2S	1/2	0	–	–	–
2	$5f^{14}6d$	^2D	3/2	3892	–	–	–
3	$5f^{14}6d$	^2D	5/2	13 559	–	–	–
4	$5f^{14}7p$	$^2P^o$	1/2	50 770	–	–	–
5	$5f^{14}7p$	$^2P^o$	3/2	75 719	–	–	–
6	$5f^{14}8s$	^2S	1/2	12 7703	–	–	–

B. Hyperfine structure of Hf I and Hf II

As it was discussed in Sec. II D, calculation of the hfs in cases when d states are involved often leads to poor accuracy of the results. This is because the density of the d states in the vicinity of the nucleus is negligible, and all values of the hfs constants come from higher-order corrections, which include mixing with s states. If leading higher-order corrections are included, then the accuracy for some states might be sufficiently good. It is important to have a way of recognizing such states. Then we would be able to recommend which states of Rf or its ions should be used to extract nuclear moments from the comparison of the measured and calculated hfs. It was suggested in Sec. II D to study partial contributions to the hfs matrix elements. It is also important to study the relative values of the higher-order corrections. In this section, we perform such a study for magnetic dipole and electric quadrupole hfs constants of Hf and Hf^+ for the states where experimental data are available. Table V shows leading and higher-order contributions to the magnetic dipole hfs constants A for five even and two odd states of Hf. Table VI shows partial wave contributions to the same A constants of the seven states of Hf; leading and higher-order contributions to the magnetic dipole

TABLE V. Contributions to the magnetic dipole hfs constants of ^{179}Hf (MHz). The CI values correspond to formula (12); HS is the difference between (13) and (12); SR is structure radiation (Fig. 2); SE is self-energy corrections (Fig. 3); TP is two-particle correction (Fig. 4). The Sum line contains the sums of all single-particle contributions (CI,HS,SR,SE). The Total line contains also TP contributions. The Final line contains error bars calculated according to (18). Experimental values are taken from [31–33].

	$^3F_2$	$^3F_3$	$^3F_4$	$^1D_2$	$^3P_2$	$^3D_2^o$	$^5G_2^o$
CI	−82.18	−35.24	−16.04	−32.38	−41.36	−42.18	191.16
HS	15.34	5.70	2.90	14.29	15.24	12.22	−52.21
SR	−13.08	−16.19	−19.67	−18.35	−13.87	−16.88	−17.80
SE	−0.90	1.70	2.66	3.13	3.28	2.50	−13.30
Sum	−80.82	−44.03	−30.15	−33.31	−36.71	−44.34	107.85
TP	11.33	−8.18	−12.69	−19.34	−25.55	−4.92	37.17
Total	−69.49	−52.21	−42.84	−52.65	−62.26	−49.26	145.02
Final	−69(7)	−52(9)	−42(9)	−52(9)	−62(14)	−49(6)	145(33)
Expt.	−71.43	−50.81	−43.46	−47.68	−44.7	−46.93	128.74

hfs constants A for five even and two odd states of Hf are taken into account. Tables VII and VIII show similar data for the electric quadrupole hfs constant B.

Studying Tables V, VI, VII, VIII, as well as Table II reveal that accurate calculated values of the hfs constants are likely to be found for the states which satisfy three conditions:

- The value of the hfs constant is relatively large.
- There is no strong cancellation between different contributions.
- The value of the hfs constant is dominated by partial contributions from the low angular momentum states.

As one can see, only magnetic dipole hfs of the ground state of Hf fully satisfies these conditions. The difference between theory and experiment, in this case, is about 3%. In all other cases, including the electric quadrupole hfs constant of the ground state, there is a large contribution from the $4d_{5/2}$ channel. However, the accuracy of the results is reasonably good for both types of the hfs constants for some other states as well. This means that the conditions above are rather most favorable than necessary conditions. On the other hand, all cases with poor results can be explained by strong cancellation between different contributions and a large contribution from the $d_{5/2}$ partial wave.

Studying Tables II, V, VI, VII, and VIII also allows one to find a way of a rough estimation of the uncertainty of the calculations and assign specific error bars to all theoretical results. Dominating contribution to the error usually comes from the contributions of the $d_{3/2}$ and $d_{5/2}$ partial waves. The data in Table II shows that the error for the $d_{3/2}$ contribution is about 10%, while the error for the $d_{5/2}$ contribution is about 20%. The contribution of the other partial waves to the error budget can be neglected because of either a small error (s and p waves) or a small contribution. It is natural to assume that the accuracy of the nondiagonal and two-particle contributions is also ∼10% since both these contributions have matrix elements with d states. Then the total error for a state a can be calculated as

$$\sigma_a = \sqrt{\sigma_{an.d.}^2 + \sigma_{ad_{3/2}}^2 + \sigma_{ad_{5/2}}^2 + \sigma_{aTP}^2}, \tag{18}$$

where $\sigma_{an.d.} = \delta_{an.d.}/10$, $\sigma_{ad_{3/2}} = \delta_{ad_{3/2}}/10$, $\sigma_{ad_{5/2}} = \delta_{ad_{5/2}}/5$, $\sigma_{TP} = \delta_{TP}/10$. Here δ stands for a particular contribution. The values of δ can be found in Tables V, VI, VII, and VIII. Error bars for the hfs constants of Hf, calculated using (18), are presented in Tables V and VII. One can see that in many cases, estimated error bars are larger than the actual difference between theory and experiment. However, in some cases of externally strong cancellations between different contributions, the estimated error bars are smaller than the difference between theory and experiment. This probably means that such states should be excluded from the consideration.

TABLE VI. Contributions of different partial waves into the magnetic dipole hfs constants of ^{179}Hf (MHz). The n.d. stands for nondiagonal contributions, which include $s_{1/2} - d_{3/2}$, $p_{1/2} - p_{3/2}$, $d_{3/2} - d_{5/2}$, etc., contributions. The TP terms are not included.

	$^3F_2$	$^3F_3$	$^3F_4$	$^1D_2$	$^3P_2$	$^3D_2^o$	$^5G_2^o$
n.d.	−37.22	0.37	23.34	27.19	8.46	−6.52	−64.55
$s_{1/2}$	18.89	−5.31	−12.34	23.69	27.71	12.46	−206.51
$p_{1/2}$	0.42	0.28	0.12	0.24	0.32	−31.63	58.40
$p_{3/2}$	0.38	0.16	0.10	−1.09	−0.31	1.94	3.61
$d_{3/2}$	-75.17	5.78	5.60	−46.41	−2.95	−41.13	177.65
$d_{5/2}$	7.92	−44.32	−44.20	−36.97	−69.08	20.59	137.18
$f_{5/2}$	2.58	0.25	−0.57	−0.27	−0.24	0.09	1.45
$f_{7/2}$	0.92	−1.01	−1.75	−0.62	−0.45	0.04	0.25
$g_{7/2}$	0.36	0.03	−0.11	0.04	0.01	−0.06	0.35
$g_{9/2}$	0.12	−0.27	0.36	−0.11	−0.18	0.03	0.01
Total	−80.82	−44.03	−30.15	-33.31	−36.71	-44.34	107.85

TABLE VII. Contributions to the electric quadrupole hfs constants of ^{179}Hf (MHz). The meaning of the contribution titles are the same as in Table V. Experimental values are taken from [31–33]. Experimental values are rounded to the last digit before decimal point. More accurate numbers together with error bars can be found in Refs. [31–33].

	$^3F_2$	$^3F_3$	$^3F_4$	$^1D_2$	$^3P_2$	$^3D^o_2$	$^5G^o_2$
CI	708	921	1972	−1107	−1358	153	2455
HS	−108	−193	−274	153	252	−155	−310
SR	130	49	33	−115	−52	99	162
SE	4	−12	−48	9	19	−11	7
Sum	734	765	1683	−1060	−1139	86	2314
TP	−2	17	57	−0.63	−22	28	80
Final	731	783	1740	−1061	−1162	114	2394
Error bar	(43)	(144)	(725)	(178)	(243)	(215)	(143)
Expt.	706	931	1619	−905	−1364	740	2802

We found experimental data on the hfs of Hf^+ for only two states, the ground state $5d6s^2\ ^2D_{3/2}$, and the excited odd state $5d6s6p\ ^4F^o_{5/2}$ [34]. Calculated contributions to the hfs of these states are presented in Table IX for the magnetic dipole hfs and Table X for the electric quadrupole hfs. One can see from Table IX that calculated A hfs constant of the ground state is consistent with zero due to strong cancellation between different contributions. On the other hand, the accuracy of the result for the excited state is high; the difference between theory and experiment is about 3%. This state satisfies all "most favorable" conditions discussed above.

For the electric quadrupole hfs constant B, the situation is opposite (see Table X); the accuracy is high for the ground state, and it is not so high for the excited state. The latter can be explained by strong cancellation between the nondiagonal contributions and the contributions from the $d_{3/2}$ partial wave.

C. Hyperfine structure of Rf I and Rf II

Hyperfine structure constants A and B calculated for selected states of Rf I and Rf II are presented in Table XI. We have calculated the hfs only for the ground state and for the low-lying states of opposite parity, which are connected to the ground state by electric dipole transitions. The frequencies of these transitions, together with the hyperfine structure, are likely to be measured first. The same method of calculations and the same analysis of the partial contributions and error bars were used for Rf I and Rf II as for Hf I and Hf II (see the previous section). We do not present tables of partial contributions for Rf I and Rf II to avoid overloading the paper with technical details. Only final results, together with the error bars, are presented in Table XI. As in the case of Hf I and Hf II the actual error of the calculations might be significantly smaller than the estimated uncertainties. Note that strong relativistic effects also pull the $7s$ and $7p_{1/2}$ electrons of Rf closer to the nucleus, enhancing their contribution to the hyperfine structure. This might be another reason for the higher accuracy of the calculation for Rf I and Rf II compared to what we had for Hf I and Hf II.

TABLE VIII. Contributions of different partial waves into the electric quadrupole hfs constants of ^{179}Hf (MHz). The n.d. stands for nondiagonal contributions, which include $s_{1/2} - d_{3/2}$, $p_{1/2} - p_{3/2}$, $d_{3/2} - d_{5/2}$, etc., contributions. The TP terms are not included.

	$^3F_2$	$^3F_3$	$^3F_4$	$^1D_2$	$^3P_2$	$^3D^o_2$	$^5G^o_2$
n.d.	865	−125	−1819	−454	144	−1117	2525
$p_{3/2}$	−5	7	26	31	−7	44	125
$d_{3/2}$	70	159	−274	294	−37	108	−19
$d_{5/2}$	−206	715	3623	−875	−1215	1041	−340
$f_{5/2}$	39	281	117	418	43	24	54
$f_{7/2}$	−56	−273	−26	−464	−80	−17	−51
$g_{7/2}$	35	48	58	77	36	0	28
$g_{9/2}$	−10	−48	−22	−87	−22	3	−8
Sum	732	765	1682	−1059	−1139	86	2314

IV. CONCLUSION

In this paper, the energy levels and the hyperfine structure constants A and B for low-lying states of the Rf atom and ions were calculated. Energy levels were calculated for Rf I, Rf II, Rf III, and Rf IV, while hyperfine structure constants were calculated for Rf I and Rf II. Similar calculations were performed for the lighter analog of Rf, the Hf atom, and its ions to control the accuracy of the calculations. Present results are in good agreement with other calculations and previous measurements where the data are available. The way of estimation of the uncertainty of the hfs calculations is suggested. For the majority of the states, the uncertainty is within 10%.

TABLE IX. Contributions into the magnetic dipole hfs constants of the $^2D_{3/2}$ and $^4F^o_{5/2}$ states of the $^{179}Hf^+$ ion (MHz). Experimental values are taken from [34].

	$^2D_{3/2}$	$^4F^o_{5/2}$		$^2D_{3/2}$	$^4F^o_{5/2}$
			n.d.	30.66	19.71
CI+HS	2.11	−521.50	$s_{1/2}$	−23.63	105.68
SR	−28.38	−0.02	$p_{1/2}$	−0.68	38.61
SE	−1.79	23.80	$p_{3/2}$	1.09	1.57
Sum	−28.06	−497.72	$d_{3/2}$	−64.44	−667.02
TP	24.06	−58.25	$d_{5/2}$	27.67	4.72
Total	−4.00	−555.97	$f_{5/2}$	1.06	−0.89
Final	−4(9)	−556(67)	$f_{7/2}$	0.07	0.00
Expt.	−17.5(0.9)	−540(2)	Total	−28.06	−497.71

TABLE X. Contributions into the electric quadrupole hfs constants of the $^2D_{3/2}$ and $^4F^o_{5/2}$ states of the $^{179}Hf^+$ ion (MHz). Experimental values are taken from [34].

	$^2D_{3/2}$	$^4F^o_{5/2}$		$^2D_{3/2}$	$^4F^o_{5/2}$
			n.d.	−342	−3228
CI+HS	1780	−897	$p_{3/2}$	6	−36
SR	63	51	$d_{3/2}$	2071	2301
SE	−32	-35	$d_{5/2}$	−9	42
Sum	1811	−881	$f_{5/2}$	34	21
TP	12	−15	$f_{7/2}$	11	−3
Total	1823	−896	$g_{7/2}$	40	23
Final	1823(208)	−896(281)	$g_{9/2}$	1	−1
Expt.	1928(21)	−728(17)	Total	1181	−881

The calculated hfs constants of Rf I and Rf II can be used to extract nuclear magnetic and electric quadrupole moments from future measurements.

ACKNOWLEDGMENTS

This work was supported by the Australian Research Council Grants No. DP190100974 and No. DP200100150. This research includes computations using the computational cluster Katana supported by Research Technology Services at UNSW Sydney [35].

TABLE XI. Hyperfine structure constants A and B for Rf I and Rf II. Numeration of states corresponds to Table IV. Error bars are calculated with the use of Eq. (18).

No.	Conf.	Term	J	Energy cm^{-1}	A/g_I MHz	B/Q MHz
				Rf I		
1	$7s^26d^2$	^3F	2	0	202(108)	271(18)
7	$7s^27p6d$	$^3D^o$	1	8028	−2546(386)	716(50)
13	$7s^27p6d$	$^3P^o$	1	16017	788(259)	−738(109)
24	$7s6d^27p$	$^5F^o$	1	25821	−14 460(1177)	−283(14)
2	$7s^27p6d$	$^3F^o$	2	2737	3185(485)	963(102)
8	$7s^27p6d$	$^3D^o$	2	11 235	−423(418)	446(129)
10	$7s^27p6d$	$^1D^o$	2	13 811	−40(150)	578(37)
9	$7s^27p6d$	$^3F^o$	3	11 328	3229(423)	1015(162)
14	$7s^27p6d$	$^3D^o$	3	17 367	939(273)	1139(217)
20	$7s6d^27p$	$^5G^o$	3	22941	5245(711)	776(54)
				Rf II		
1	$7s^26d$	^2D	3/2	0	−190(137)	1448(130)
5	$7s^27p$	$^2P^o$	1/2	19 050	12 960(280)	0
14	$7s7p6d$	$^4D^o$	1/2	37 378	−21 730(2636)	0
13	$7s^27p$	$^2P^o$	3/2	33 621	−7798(849)	2078(113)
15	$7s7p6d$	$^2P^o$	3/2	40 015	7193(937)	1414(28)
10	$7s7p6d$	$^4F^o$	3/2	30 264	9650(984)	1374(43)
12	$7s7p6d$	$^4F^o$	5/2	33 320	15 810(1828)	417(141)
16	$7s7p6d$	$^4D^o$	5/2	40 640	7582(1532)	1421(259)

[1] Y. T. Oganessian, V. K. Utyonkov, Y. V. Lobanov *et al.*, Heavy element research at Dubna, Nucl. Phys. A **734**, 109 (2004).
[2] Y. Oganessian, Heavy element research at FLNR (Dubna), Eur. Phys. J. A **42**, 361 (2009).
[3] Y. Oganessian, Nuclei in the "Island of Stability" of superheavy elements, Acta Phys. Pol. B **43**, 167 (2012).
[4] J. H. Hamilton, S. Hofmann, and Y. T. Oganessian, Search for superheavy nuclei, Annu. Rev. Nucl. Part. Sci **63**, 383 (2013).
[5] M. Leino, Production and properties towards the island of stability, EPJ Web Conf. **131**, 01002 (2016).
[6] M. Laatiaoui, W. Lauth, H. Backe *et al.*, Atom-at-a-time laser resonance ionization spectroscopy of nobelium, Nature (London) **538**, 495 (2016).
[7] S. Raeder, D. Ackermann, H. Backe, R. Beerwerth, J. C. Berengut, M. Block, A. Borschevsky, B. Cheal, P. Chhetri, C. E. Dullmann *et al.*, Probing Sizes and Shapes of Nobelium Isotopes by Laser Spectroscopy, Phys. Rev. Lett. **120**, 232503 (2018).
[8] S. G. Porsev, M. S. Safronova, U. I. Safronova, V. A. Dzuba, and V. V. Flambaum, Nobelium energy levels and hyperfine-structure constants, Phys. Rev. A **98**, 052512 (2018).
[9] E. V. Kahl, J. C. Berengut, M. Laatiaoui, E. Eliav, and A. Borschevsky, High-precision *ab initio* calculations of the spectrum of Lr^+, Phys. Rev. A **100**, 062505 (2019).
[10] B. R. J. Muhyedeen, The Quantized Atomic Masses of the Elements: Part-6; Z=100-107 (Fm-Bh), Euro. J. Sci. Res. **152**, 418 (2019).
[11] E. Eliav, U. Kaldor, and Y. Ishikawa, Ground State Electron Configuration of Rutherfordium: Role of Dynamic Correlation, Phys. Rev. Lett. **74**, 1079 (1995).
[12] N. S. Mosyagin, I. I. Tupitsin, and A. V. Titov, Precision calculation of the low-lying excited states of the Rf atom, Radiochemistry **52**, 394 (2010).
[13] V. A. Dzuba, M. S. Safronova, and U. I. Safronova, Atomic properties of superheavy elements No, Lr, and Rf, Phys. Rev. A **90**, 012504 (2014).
[14] V. A. Dzuba, Combination of the single-double coupled-cluster and the configuration-interaction methods: Application to barium, lutetium, and their ions, Phys. Rev. A **90**, 012517 (2014).
[15] V. A. Dzuba, V^{N-M} approximation for atomic calculations, Phys. Rev. A **71**, 032512 (2005).
[16] W. R. Johnson and J. Sapirstein, Computation of Second-Order Many-Body Corrections in Relativistic Atomic Systems, Phys. Rev. Lett. **57**, 1126 (1986).
[17] W. R. Johnson, S. A. Blundell, and J. Sapirstein, Finite basis sets for the Dirac equation constructed from B splines, Phys. Rev. A **37**, 307 (1988).
[18] V. A. Dzuba, V. V. Flambaum, P. G. Silvestrov, and O. P. Sushkov, Correlation potential method for the calculation of energy levels, hyperfine structure and E1 transition amplitudes in atoms with one unpaired electron, J. Phys. B **20**, 1399 (1987).
[19] V. A. Dzuba, J. C. Berengut, C. Harabati, and V. V. Flambaum, Combining configuration interaction with perturbation theory for atoms with a large number of valence electrons, Phys. Rev. A **95**, 012503 (2017).
[20] V. A. Dzuba, V. V. Flambaum, M. G. Kozlov, and S. G. Porsev, Using effective operators in calculating the hyperfine structure of atoms, J. Exp. Theor. Phys. **87**, 885 (1998).

[21] V. A. Dzuba and V. V. Flambaum, Off-diagonal hyperfine interaction and parity nonconservation in cesium, Phys. Rev. A **62**, 052101 (2000).

[22] L.-J. Ma and G. zu Putlitz, On the electric nuclear quadrupole moments of ^{135,137}Ba, Z. Phys. A **277**, 107 (1976).

[23] R. E. Silverans, G. Borghs, P. De Bisschop, and M. Van Hove, Hyperfine structure of the 5d ^{2}D$_J$ states in the alkaline-earth Ba ion by fast-ion-beam laser-rf spectroscopy, Phys. Rev. A **33**, 2117 (1986).

[24] H. Ramanantoanina, A. Borschevsky, M. Block, and M. Laatiaoui, Electronic structure of $Rf^+(Z = 104)$ from *ab initio* calculations, Phys. Rev. A **104**, 022813 (2021).

[25] M. S. Safronova, M. G. Kozlov, W. R. Johnson, and D. Jiang, Development of a configuration-interaction plus all-order method for atomic calculations, Phys. Rev. A **80**, 012516 (2009).

[26] V. V. Flambaum and J. S. M. Ginges, Radiative potential and calculations of QED radiative corrections to energy levels and electromagnetic amplitudes in many-electron atoms, Phys. Rev. A **72**, 052115 (2005).

[27] V. A. Dzuba, M. S. Safronova, U. I. Safronova, and A. Kramida, Ionization potentials of superheavy elements No, Lr, and Rf and their ions, Phys. Rev. A **94**, 042503 (2016).

[28] E. Johnson, B. Fricke, O. L. Keller, Jr., C. W. Nestor, Jr., and T. C. Tucker, Ionization potentials and radii of atoms and ions of element 104 (unnilquadium) and of hafnium (2+) derived from multiconfiguration Dirac–Fock calculations, J. Chem. Phys. **93**, 8041 (1990).

[29] A. Kramida, Yu. Ralchenko, J. Reader, and NIST ASD Team, NIST Atomic Spectra Database (Version 5.7.1), [https://physics.nist.gov/asd] (National Institute of Standards and Technology, Gaithersburg, 2019).

[30] P. F. A. Klinkenberg, T. A. M. Van Kleef, and P. E. Noorman, Structure and Ionization Potential of Hf III and Hf IV, Physica **27**, 151 (1961).

[31] S. Büttgenbach, R. Dicke, and H. Gebauer, Hyperfine structure of the $5d^26s^2\ ^3F_{3,4}$ metastable atomic levels of ^{179}Hf and the nuclear quadrupole moments of ^{177}Hf and ^{179}Hf, Phys. lett. A **62**, 307 (1977).

[32] N. Boos, F. Le Blanc, M. Krieg, J. Pinard, G. Huber, M. D. Lunney, D. LeDu, R. Meunier, M. Hussonnois, O. Constantinescu *et al.*, Nuclear Properties of the Exotic High-Spin Isomer $^{178}Hf^{m2}$ from Collinear Laser Spectroscopy, Phys. Rev. Lett. **72**, 2689 (1994).

[33] D. Zimmermann, P. Baumann, D. Kuszner, and A. Werner, Isotope shift and hyperfine structure in the atomic spectrum of hafnium by laser spectroscopy, Phys. Rev. A **50**, 1112 (1994).

[34] W. Z. Zhao, F. Buchinger, J. E. Crawford, S. Fedrigo, S. Gulick, J. K. P. Lee, O. Constantinescu, M. Hussonnois, and J. Pinard, Hyperfine structure and isotope shifts in the $5d6s^2\ a^2D_{3/2}-5d6s(a^3D)6p\ z^4F^o_{5/2}$ transition of Hf II, Hyperfine Interact. **108**, 483 (1997).

[35] Katana (shared computational cluster), [https://doi.org/10.26190/669x-a286], University of New South Wales, Sydney, 2010.